ISSN 1330-3651 (Print), ISSN 1848-6339 (Online)
UDC/UDK 621.783.23-477:539.377.384.388]:519.6

ANALYTICAL AND NUMERICAL STRESS ANALYSIS OF THE ROTARY KILN RING

Alma Žiga, Aleksandar Karač, Dušan Vukojević

Original scientific paper
This paper presents an analysis of the stress distribution on the outer surface of the riding ring of rotary cement kiln during working cycle using both the theory and finite element simulation. In the theoretical analysis, the total stress is obtained as a combination of bending, thermal and contact stresses. To obtain bending stress the kiln is considered as a simply supported, indeterminate beam subjected to static and symmetrical loads and Castigliano's theorem is employed. Thermal stresses are obtained assuming both linear and non-linear temperature distribution over the ring thickness. Contact stress between ring and supporting rollers is obtained using Hertz contact theory. Bending, thermal and contact stresses are also obtained numerically in separate simulations, mimicking conditions assumed in the theoretical part. All results are in excellent agreement. In addition, a more realistic ring model subjected to all loads simultaneously is also simulated. These results showed slight disagreement with theory in the contact region, mainly due to sliding contact between the roller and the ring, but overall agreement was good.

Keywords: *bending stress, contact stress, kiln ring, thermal effects*

Analitička i numerička analiza naprezanja u nosivom prstenu rotacijske peći

Izvorni znanstveni članak
Ovaj rad predstavlja analizu raspodjele naprezanja na vanjskoj površini nosivog prstena rotacijske peći u radnom ciklusu uporabom teorijske analize i simulacije metodom konačnih elemenata. U teorijskoj analizi, ukupno naprezanje je dobiveno kombinacijom savojnog naprezanja, toplinskih i kontaktnih naprezanja. Za dobivanje savojnog naprezanja, peć se promatra kao prosta, statički neodređena greda koja je opterećena statičkim i simetričnim opterećenjima, pri čemu se koristi Castiglianov teorem. Toplinska naprezanja dobivena su pretpostavljajući i linearnu i nelinearnu raspodjelu temperature kroz debljinu prstena. Konstantna naprezanja između prstena i nosivih valjaka dobivena su uporabom Hertzove teorije za kontaktna naprezanja. Naprezanja uslijed savijanja, toplinska i kontaktna naprezanja dobivena su i numerički u odvojenim simulacijama, u kojima su korišteni uvjeti usvojeni u teorijskom dijelu. Svi se rezultati odlično slažu. Pored toga, simuliran je i realniji model prstena koji je izložen svim naprezanjima istovremeno. Ovi rezultati pokazali su manja odstupanja od teorije, naročito zbog klizajućeg kontakta između prstena i nosivih valjaka, ali se općenito dobro slažu.

Ključne riječi: *kontaktno naprezanje, noseći prsten, savijanje, toplinski efekti*

1 Introduction

Riding rings are supporting elements of rotary kilns, and as such are subjected to various dynamic stresses. These stresses are caused by loads from the kiln weight and row-mix feed, rotation of the kiln and by temperature gradients. In order to predict ring behaviour and estimate its service life it is essential to calculate these stresses as accurately as possible.

There are a limited number of studies in literature that examine stress state of rotary kiln rings in more details. Maziarz and Tasak [5] studied fatigue failure of the rings and gave simplified equations for bending stresses caused by continuous load; detailed analysis of contact and thermal stresses was omitted. Similar analysis was carried out by Xiao et al. [6], who investigated contact pressure distribution and support angle optimisation of the kiln ring, however they also did not include temperature effects. Bowen and Saxer [7] investigated causes and effects of kiln ring problems and included thermal stresses, but the analysis of bending stresses due to continuous load was simplified. In addition, there are numerous studies investigating the rotary kiln stresses, stresses in supporting rollers, heat transfer in the kiln, etc. [8 ÷ 11], but to the authors' knowledge, there are no published studies with detailed theoretical investigation and numerical simulation of the kiln ring.

This paper focuses on detailed analytical analysis of the kiln ring stresses caused by continuous loads, contact between the ring and the roller and by temperature gradients and numerical simulation of the same problem. To this end, the rotary kiln of the cement plant in Kakanj, shown in Fig. 1, is considered. It is a 70 m long steel tube with inner diameter of 4,6 m and slope of 3,5°, and rotation speed of 2 rpm. The mass of the kiln, including refractory line and feed, is around 1000 t and is supported by three ring-roller stations, spaced along the length of the kiln. The main dimensions and properties of the kiln necessary for subsequent analysis are given in Tab. 1.

Figure 1 Rotary kiln in the cement plant in Kakanj

Table 1 Rotary kiln data (in mm)

Ring	Inner radius, R_1	Outer radius, R_2	Width, B
Ring 1	2318	2700	750
Ring 2, 3	2323	2700	880

Distributed loads along the kiln length:

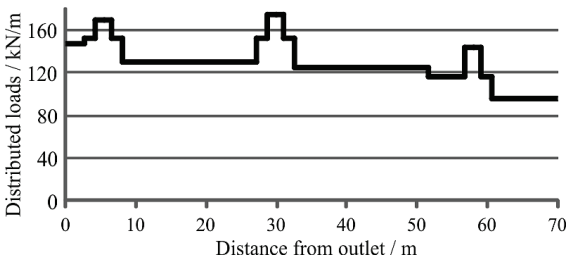

2 Support reactions in the kiln ring

In order to calculate support reactions in the kiln rings, the kiln is divided into 17 segments, due to different shell rigidity, supports and drive-gear positions, and distributed loads, as shown in Fig. 2. The kiln is modelled in MdSolids3.2 software with the following assumptions:

- Raw-mix in kiln is evenly distributed along kiln length with specific weight of 18,58 kN/m,
- Raw-mix is symmetrically distributed around vertical axis of kiln (Fig. 3),
- Temperature does not affect shell rigidity,
- Specific weight of line bricks on inlet side (18,2 m), i.e. right-hand side in Fig. 2, is 44 kN/m. The remaining part of the kiln has line bricks with specific weight of 74 kN/m. Distributed loads in Fig. 2 correspond to the graph in Tab. 1. Weight of the gear ring is F_g= 353 kN.

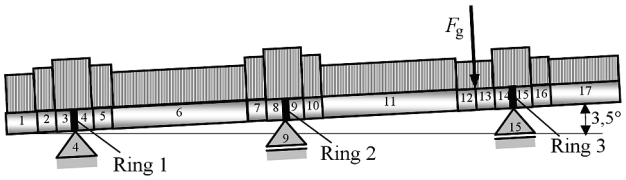

Figure 2 Kiln model

As a results of the analysis, the following roller support reactions, namely nodes 4, 9 and 15, are obtained: F_4=2183,7 kN, F_9=4013,86 kN and F_{15}=3154 kN. Using the highest value, in the middle roller station, one can obtain the maximum load Q, acting on the ring (see Fig. 3) as $Q = \frac{F_9}{2\cos 30°}$.

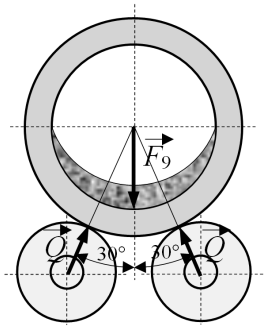

Figure 3 Roller stations with reactions

3 Analytical solutions

Stress distribution in the riding ring can be obtained as a combination of bending, contact and thermal stresses acting on the ring, as a result of distributed load in the kiln, contact between rollers and the ring, and temperature gradient. In this work, bending stresses are obtained following the work by Maziarz and Tasak [5] and Xiao et al. [6], where basic equations are given together with boundary conditions applied in order to obtain bending moments. Contact stresses between kiln rollers and the kiln ring are obtained using classical Hertzian contact analysis [1]. Thermal stresses are calculated using expressions given by Timoshenko [2] and Bowen and Saxer [7].

3.1 Bending stresses due to continuous load

In order to obtain distribution of bending stresses, it is necessary to calculate bending moments in each cross section of the ring. To this end, three regions of the ring can be distinguished, as shown in Fig. 4 (only a half of the ring is considered in the analysis due to symmetry): region I for $0 \leq \varphi \leq \pi/2$, region II for $\pi/2 \leq \varphi \leq 5\pi/6$ and region III for $5\pi/6 \leq \varphi \leq \pi$. It is assumed here that the continuous load acts from $\varphi=\pi/2$, and is described by the following function of φ:

$$q = \frac{2F}{R_1\pi}\cos\varphi\,, \tag{1}$$

Now, according to Fig. 4, we have bending moments:
(i) Region I:

$$M_b = M_0 + N_0 R_{avg}(1-\cos\varphi), \tag{2}$$

(ii) Region II:

$$M_b = M_0 + N_0 R_{avg}(1-\cos\varphi) + M_q\,, \tag{3}$$

(iii) Region III:

$$M_b = M_0 + N_0 R_{avg}(1-\cos\varphi) + M_q - QR_{avg}\sin\left(\varphi - \frac{5\pi}{6}\right), \tag{4}$$

where the moment of distributed load M_q, is given by:

$$M_q = \int_{\frac{\pi}{2}}^{\varphi} q\cdot R_1 \mathrm{d}\psi \cdot R_{avg}\sin(\varphi-\psi) = \\ = \int_{\frac{\pi}{2}}^{\varphi} \frac{2F}{R_1\pi}(\cos\psi)R_1\cdot R_{avg}\sin(\varphi-\psi)\,\mathrm{d}\psi\,, \tag{5}$$

$$M_q = -\frac{FR_{avg}\left[-2\cos\varphi + (\pi-2\varphi)\sin\varphi\right]}{2\pi}, \tag{6}$$

and R_{avg}=0,5·(R_1+R_2) is the mean radius of the ring, and R_1 and R_2 are inner and outer radius of the ring, respectively.

Bending moment M_0 and horizontal force N_0 can be obtained using Castigliano's theorem, i.e. via partial derivatives of the strain energy in the ring with respect to M_0 and N_0. Here, the strain energy can be considered as a function of bending moment only, since the contributions of direct tensile and shear forces can be neglected in the presence of bending [4], and is given by

$$U = \frac{R_{avg}}{EI}\int_0^{\pi} M_b^2 \mathrm{d}\varphi\,. \tag{7}$$

Now, by applying Castigliano's theorem, with the angle of rotation, α, and the horizontal displacement, δ, of the cross section A of the ring equal to zero, we have

$$\alpha\big|_{\varphi=0} = \frac{\partial U}{\partial M_0}\bigg|_{\varphi=0} = \frac{R_{\text{avg}}}{EI}\int_0^{\pi} 2M_{\text{b}}\frac{\partial M_{\text{b}}}{\partial M_0}\,\text{d}\varphi = 0\,, \tag{8}$$

and

$$\delta\big|_{\varphi=0} = \frac{\partial U}{\partial N_0}\bigg|_{\varphi=0} = \frac{R_{\text{avg}}}{EI}\int_0^{\pi} 2M_{\text{b}}\frac{\partial M_{\text{b}}}{\partial N_0}\,\text{d}\varphi = 0\,. \tag{9}$$

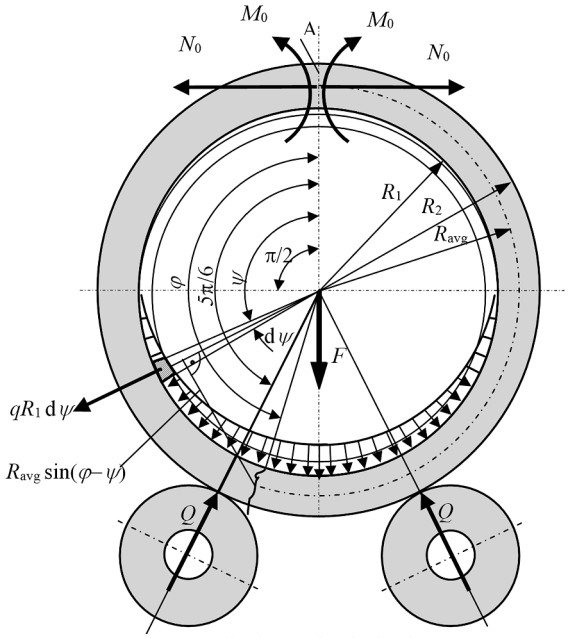

Figure 4 Kiln ring under the load [5]

After integration, equations (8) and (9) become:

$$M_0\pi + N_0 R_{\text{avg}}\pi + F\left(\frac{2R_{\text{avg}}}{\pi} - \frac{R_{\text{avg}}}{\sqrt{3}}\right) = 0\,, \tag{10}$$

and

$$M_0\pi + \frac{3R_{\text{avg}}\pi}{2} + \frac{FR_{\text{avg}}}{72}\left(9 - 24\sqrt{3} + \frac{144}{\pi} - \sqrt{3}\pi\right) = 0\,. \tag{11}$$

By solving equations (10) and (11), the final expressions for the unknown internal moment M_0 and internal force N_0 are obtained:

$$N_0 = \frac{F(\sqrt{3}\pi - 9)}{36\pi}, \tag{12}$$

$$M_0 = -\frac{FR_{\text{avg}}(72 - 9\pi - 12\sqrt{3}\pi + \sqrt{3}\,\pi^2)}{36\pi^2}\,. \tag{13}$$

In order to obtain circumferential stresses at the outer surface, the ring can be considered as a curved bar and the following expression can be applied [3]:

$$\sigma_{\text{b}} = \frac{M_{\text{b}}(R_{\text{n}} - R_2)}{AR_2(R_{\text{avg}} - R_{\text{n}})}, \tag{14}$$

where $R_{\text{n}}=(R_2-R_1)/\ln(R_2/R_1)$ is the distance of neutral axis of the ring cross section from the central axis of the ring and A is the area of the ring cross section. It is worth of noting that in literature, e.g. [5 ÷ 7], the kiln is usually considered a straight beam and a simplified expression, $\sigma_{\text{b}}=M_{\text{b}}/W$, is used to obtain bending stresses, where $W=B\cdot H^2/6$ is the section modulus. The difference between two approaches is 5 % for the case considered.

Now, using equations (2), (3) and (4) one can obtain circumferential stress distribution at the outer surface of the kiln ring as a function of φ, as shown in Fig. 5. As can be seen, in one full cycle the ring goes twice through two extreme tensile stresses, at around 107° and at 180°, and twice through two extreme compressive stresses, at 0° and at contact region with rollers (150°), with maximum tensile stress at 107° and maximum compressive stress in the contact region with the roller. Nevertheless, the magnitude of these stresses is well below critical values.

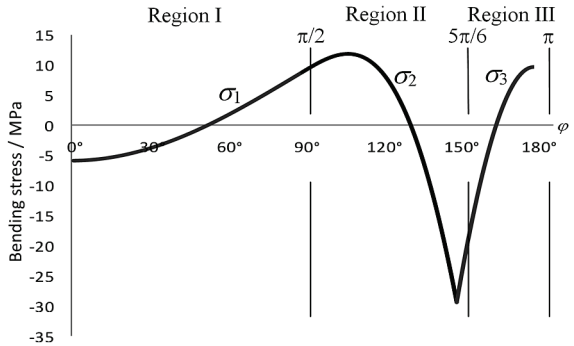

Figure 5 Bending stress at the outer surface of the ring

3.2 Thermal stress in the ring

The general expression for circumferential stress in the ring due to temperature field is obtained from [2]:

$$\sigma_t = \frac{E}{1-\mu}\left[\frac{1}{r^2}\int_{R_1}^{r}\alpha_l t\cdot r\,\text{d}r + \frac{r^2 + {R_1}^2}{r^2\left({R_2}^2 - {R_1}^2\right)}\int_{R_1}^{R_2}\alpha_l t\cdot r\,\text{d}r - \alpha_l t\right], \tag{15}$$

where α_l is the coefficient of linear expansion, t is the temperature distribution over the ring thickness, E is the modulus of elasticity and μ is Poisson's ratio.

For a thin-wall ring with inside temperature t_{i} and outside temperature t_{o} ($t_{\text{i}} > t_{\text{o}}$, Fig. 6), the steady-state temperature over the thickness is almost linear and can be approximated by:

$$t = t_{\text{o}} + \Delta T\frac{R_2 - r}{R_2 - R_1}, \tag{16}$$

where $\Delta T = t_{\text{i}} - t_{\text{o}}$ is the temperature difference. By substituting equation (16) into (15), one can obtain final expression for circumferential stress distribution through ring thickness. For the outer surface, $r=R_2$, circumferential stress is positive and can be calculated using the following expression [7]:

$$\sigma_t = \frac{E\cdot\alpha_l\cdot\Delta T}{3(1-\mu)}\cdot\frac{m+2}{m+1}, \tag{17}$$

where m is the ratio of outside and inside radius of the ring, i.e. $m = R_2 / R_1$.

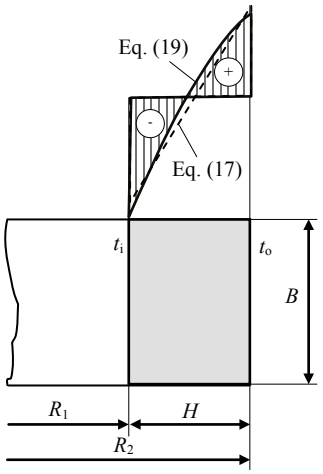

Figure 6 Temperature distributions through ring thickness

Under adopted assumptions, the thermal stress at the outer surface is constant circumferentially, and is equal to 175 MPa for the case considered.

On the other hand, if the thickness of the wall is not considered small, temperature distribution is not linear and may be represented by the function:

$$t = \frac{\Delta T}{\ln \frac{R_2}{R_1}} \cdot \ln \frac{R_2}{r} + t_o , \tag{18}$$

leading to the following expression for circumferential thermal stress:

$$\sigma_t = \frac{E\alpha_l \cdot \Delta T}{2(1-\mu)} \cdot \frac{1+m^2+2\ln m}{(1-m^2)\cdot \ln m} . \tag{19}$$

This expression produces thermal stress of 171 MPa, with approximately 2,3 % difference with the case of thin-wall ring assumption.

3.3 Contact stress in the ring

Pressure distribution due to contact between the roller and the ring, assumed here as a full circle, has a semi-elliptical distribution, with the maximum contact stress in the middle of the contact area [1]:

$$\sigma_{c\,max} = \frac{2Q}{\pi a B} , \tag{20}$$

where Q is the normal force acting on the ring (Fig. 3 and 4), a is a half-width of the contact area:

$$a = \sqrt{\frac{4QR}{\pi B E^*}} , \tag{21}$$

R is the equivalent radius $1/R = (1/R_1+1/R_2)$, E^* is the equivalent modulus of elasticity $1/E^* = ((1-\mu^2)/E_1 + (1-\mu^2)/E_2)$, and indices 1 and 2 relate to the ring and the roller, respectively, and B is the contact width. Maximum contact (compressive) stress occurs twice in one revolution and equals 396 MPa.

4 Numerical analysis

Numerical analysis is carried out using ABAQUS software [12]. In all simulations the ring and rollers (where applied) are modelled in 2D, with only a half of the domain modelled due to symmetry and plain strain condition is applied. Simulations are considered steady-state, i.e. inertia effects are neglected due to slow rotation of the kiln. Material properties for both parts are those of steel. Firstly, the ring is subjected to individual loads as employed in the analytical section, and results are compared with analytical solutions. Then, a more realistic model, with all loading conditions acting simultaneously, is simulated and analysed.

4.1 Bending stresses due to continuous load

Fig. 7 shows the meshed ring model with boundary conditions. The ring is meshed using 8414 linear quadrilateral elements of type CPE4T and 60 linear triangular elements of type CPE3T. Contact region between the roller and the ring in this simulation is simplified by a simple pinned support, i.e. movement is constrained in the x and y directions. Load distribution is applied along the lower internal circumference of the ring using a user-defined subroutine DLOAD with Eq. (1) employed. Outer and internal upper half surfaces are stress-free and right cross-sectional surfaces are symmetry planes.

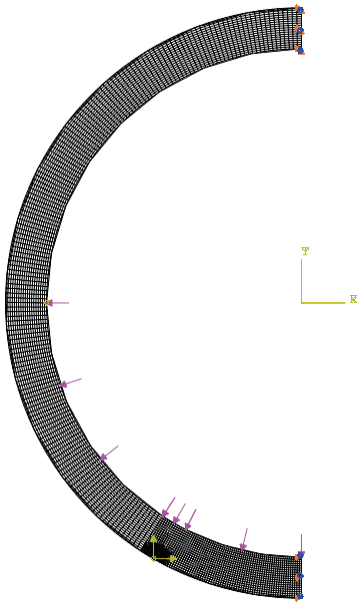

Figure 7 The ring model subjected to continuous load

Fig. 8 shows comparison of bending stresses at the outer ring surface obtained analytically and numerically. It is clear that agreement is very good, with maximum difference of 5 % in the region of maximum tensile stress (107°) and at 0°. The region around support is not plotted

due to high stress peaks in the numerical simulations caused by fixed point support.

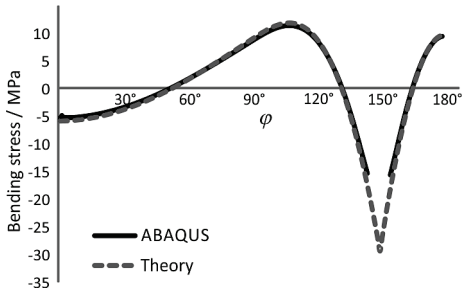

Figure 8 Bending stresses due to continuous load

4.2 Thermal stress in the ring

In order to simulate conditions used in Section 3.2 and obtain thermal stresses numerically, the ring, with the mesh as in Section 4.1 without support, is subjected to constant temperatures at the outer (t_o) and inner (t_i) surfaces, using fixed value boundary condition. As a result, constant circumferential tensile stress of 170,8 MPa at the outer surface is obtained, which is very close to the thick-ring assumption and non-linear temperature distribution in the ring (Eq. 19).

4.3 Contact stress in the ring

Contact stresses are obtained numerically using the model given in Fig. 9. Here, the ring and roller are modelled as full cylinders to accommodate assumptions used in the analytical solution. Only a quarter of each part is modelled and the force Q (Fig. 3) is applied to the roller (upper cylinder) as shown in Fig. 9.

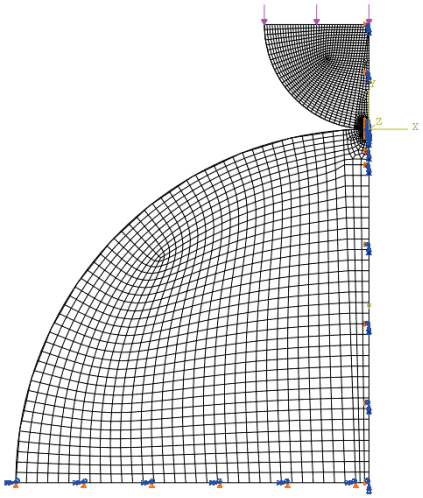

Figure 9 Contact between roller and the ring – simplified analysis

The mesh consists of 4141 CPE4R elements for the ring and 4909 CPE4R elements for the roller, with refined mesh in the region of contact to obtain more accurate results. Outside boundaries are modelled as stress-free, with bottom and right boundaries as symmetry planes. Contact between the roller and the ring is modelled using frictionless formulation. The type of interaction between ring and rollers is surface-to-surface with small sliding formulation and surface-to-surface discretisation method. As a result of this simulation, maximum (compressive) contact stress of 396 MPa is obtained in the middle of contact area, the same as analytically.

4.4 The ring-roller system – simultaneous loading conditions

The meshed ring-roller system with proper contact between parts, subjected to the temperature gradient as in Section 3.2 and loading given in Section 3.1 is shown in Figure 10. Coupled temperature-displacement step type is chosen for the analysis with steady-state response. Domain is meshed using linear quadrilateral CPE4T and triangular elements CPE3T; total number of elements is 23657 of CPE4T and 126 of CPE3T. Similarly to contact analysis in previous section, mesh is refined in the contact region to get better accuracy. Contact is simulated using penalty friction formulation with coefficient of friction equal to 0,1, and surface-to-surface interaction with finite sliding formulation between parts.

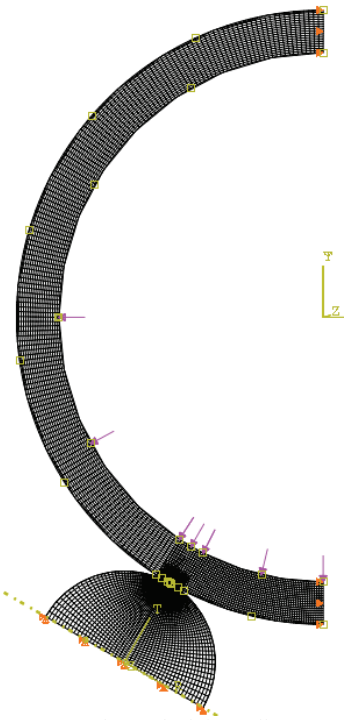

Figure 10 The meshed ring-roller system

Fig. 11 shows circumferential stress distribution in the ring and the roller. It can be observed that the profile is very similar, i.e. linear through thickness, to that caused by temperature gradient in the most of the ring domain. However, a closer look at the contact region reveals significant deviation from the overall trend due to contact stresses.

Circumferential stress distribution at the outer surface is given in Fig. 12. It is clear that the ring is subjected to the almost constant stress of 175 MPa, caused by temperature gradient, with two stress peaks in each rotation, caused by contact between the ring and the roller. On the other hand, the effects of bending stresses are minor. Overall agreement with analytical solution is good. However, it is clear that the analytical solution significantly overestimates compressive stresses in the

contact region, mainly due to simplified boundary conditions in the analytical approach.

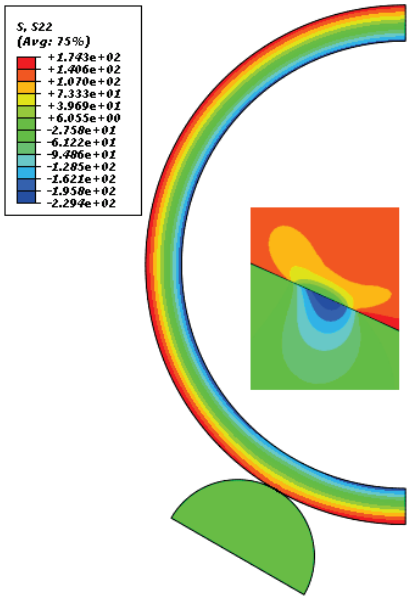

Figure 11 Circumferential stress distribution in the ring and rollers

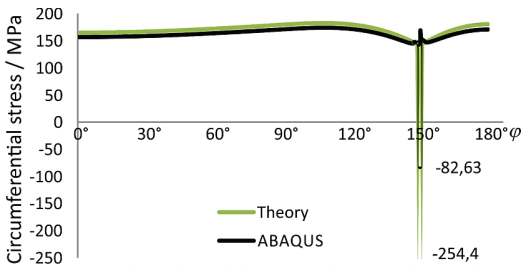

Figure 12 Circumferential stress at the outer ring surface

5 Conclusions

Circumferential stresses of the kiln ring caused by distributed loads, contact with supporting rollers and temperature gradients are analysed analytically and numerically. A good overall agreement between two approaches is obtained. However, numerical analysis of a more realistic kiln-ring system revealed smaller compressive stresses in the contact region compared to the analytical predictions. The major contribution to the total stress is that of temperature gradients, causing almost constant stress in the outer surface of the ring. Stress magnitudes are well below yield stress of the ring material, so the linear-elastic analysis employed in this study suffices.

6 References

[1] Johnson, K. L. Contact Mechanics, Cambridge University Press, Cambridge, 1985.
[2] Timoshenko, S. Strength of Materials, part II, Advanced Theory and Problems, D. Van Nostrand Company, New York, 1942.
[3] Hibbeler, R. C. Mechanics of Materials, eighth edition, Pearson Prentice Hall, 2011.
[4] Young, W. C.; Budynas, R. G. Roark's Formulas for Stress and Strain, Seventh Edition, McGraw-Hill, 2002.
[5] Maziarz, M.; Tasak, E. Case study of fatigue failures in the support rings of a cement kiln. //International Journal of Fatigue. 2, 3(1992), pp. 84-90.
[6] Xiao, Y.; Pan, D.; Lei, X. Contact pressure distribution and support angle optimization of kiln tyre. // J. Cent. South Univ. Technol. 13, 3, 6(2006), pp. 246-250.
[7] Bowen A. E.; Saxer, B. Causes and effect of kiln tyre problems. // IEEE transaction on industry applications. IA-21, 2, 3(1985), pp. 344-355.
[8] Pazand, K.; Shariat Panahi, M.; Pourabdoli, M. Simulating the mechanical behaviour of a rotary cement kiln using artificial neural networks. // Materials and Design. 30, (2009), pp. 3468-3473.
[9] del Coz Diaz, J. J.; Rodriguez Mazon, F.; Garcia Nieto, P. J.; Suarez Dominguez, F. J. Design and finite element analysis of a wet cycle cement rotary kiln. // Finite Elements in Analysis and Design. 39, (2002), pp. 17-42.
[10] Chen, Z.; Zeng, F.; Fan, T.; Xiao, J.; Shen, J. Numerical analysis of static stress on the body of 10000 t/d rotary kiln's main body. // International Conference on Experimental Mechanics 2008, edited by Xiaoyuan H., Humin X., Yilan K.
[11] Sonavane, Y.; Specht, E. Numerical analysis of the heat transfer in the wall of rotary kiln using finite element method ANSYS, Seventh International Conference on CFD in the Minerals and Process Industries CISRO, Melbourne, Australia, 2009.
[12] ABAQUS 6.9-1, commercial FEA Software, product of Dassault Systèmes Simulia Corp., Providence, RI, USA.

Authors' addresses

Alma Žiga, M. Sc., Assistant
Faculty of Mechanical Engineering
Fakultetska 1, 72 000 Zenica
Bosnia and Herzegovina
E-mail: aziga@mf.unze.ba

Aleksandar Karač, PhD, Associate professor
Faculty of Mechanical Engineering
Fakultetska 1, 72 000 Zenica
Bosnia and Herzegovina
E-mail: akarac@mf.unze.ba

Dušan Vukojević, PhD, Professor
Faculty of Mechanical Engineering
Fakultetska 1, 72 000 Zenica
Bosnia and Herzegovina
E-mail: dvukojevic@mf.unze.ba